Regulatory R region of the CFTR chloride channel is a dynamic integrator of phospho-dependent intra- and intermolecular interactions

Zoltan Bozoky[a,b], Mickael Krzeminski[a,b], Ranjith Muhandiram[b], James R. Birtley[c], Ateeq Al-Zahrani[c,1], Philip J. Thomas[d], Raymond A. Frizzell[e], Robert C. Ford[c], and Julie D. Forman-Kay[a,b,2]

[a]Program in Molecular Structure and Function, Hospital for Sick Children, Toronto, ON, Canada M5G 1X8; [b]Department of Biochemistry, University of Toronto, Toronto, ON, Canada M5S 1A8; [c]Faculty of Life Sciences, University of Manchester, Manchester M13 9PT, United Kingdom; [d]Department of Cell Biology and Physiology, University of Pittsburgh School of Medicine, Pittsburgh, PA 15261; and [e]Department of Physiology, University of Texas Southwestern Medical Center, Dallas, TX 75390

Edited by Peter E. Wright, The Scripps Research Institute, La Jolla, CA, and approved October 8, 2013 (received for review September 9, 2013)

Intrinsically disordered proteins play crucial roles in regulatory processes and often function as protein interaction hubs. Here, we present a detailed characterization of a full-length disordered hub protein region involved in multiple dynamic complexes. We performed NMR, CD, and fluorescence binding studies on the nonphosphorylated and highly PKA-phosphorylated human cystic fibrosis transmembrane conductance regulator (CFTR) regulatory region, a ∼200-residue disordered segment involved in phosphorylation-dependent regulation of channel trafficking and gating. Our data provide evidence for dynamic, phosphorylation-dependent, multisite interactions of various segments of the regulatory region for its intra- and intermolecular partners, including the CFTR nucleotide binding domains 1 and 2, a 42-residue peptide from the C terminus of CFTR, the SLC26A3 sulphate transporter and antisigma factor antagonist (STAS) domain, and 14-3-3β. Because of its large number of binding partners, multivalent binding of individually weak sites facilitates rapid exchange between free and bound states to allow the regulatory region to engage with different partners and generate a graded or rheostat-like response to phosphorylation. Our results enrich the understanding of how disordered binding segments interact with multiple targets. We present structural models consistent with our data that illustrate this dynamic aspect of phospho-regulation of CFTR by the disordered regulatory region.

protein interaction network | fuzzy complex

Intrinsically disordered proteins (IDPs) and intrinsically disordered protein regions compose a large portion of the higher eukaryotic proteome (1) and lack stable secondary and tertiary structures under physiological conditions (2). IDPs play a dominant role in mediating interactions with other proteins, leading to their significant involvement in signaling and regulatory functions. A flexible chain facilitates interaction with many partner surfaces; therefore, IDPs often have several binding partners and are overrepresented among hub proteins (3–5). The entropic cost of IDP binding can lead to low-affinity but high-specificity interactions (6). Affinities can be modulated by posttranslational modifications, such as phosphorylation, and these modifications are highly correlated with protein disorder (7), enabling control of protein function, localization, and turnover (7, 8).

In most globular proteins, multiple segments contribute to one interaction surface, whereas binding is often localized to a single continuous segment of an IDP called a binding motif (9). Disordered proteins, particularly IDPs with hub functions, can display multiple, often overlapping sites for different partners (4, 10). A binding partner can select a conformation from the IDP ensemble that exists before the interaction (conformational selection) or induce a novel conformation on binding (induced fit), with both mechanisms playing a role in the formation of many IDP complexes (11, 12). The resulting complexes can become completely ordered or remain dynamic (or fuzzy). In such complexes, the bound IDP fluctuates between various structures, providing accessibility for other partners or posttranslational modifications (13, 14).

Cystic fibrosis (CF) is caused by mutations in the CF transmembrane conductance regulator (CFTR). The intrinsically disordered regulatory (R) region of CFTR controls the gating and trafficking of this chloride channel in a phosphorylation-dependent manner. In the nonphosphorylated state, the channel is closed, and phosphorylation (15) or removal (16, 17) of the R region leads to channel opening. In addition to phosphorylation, ATP binding and hydrolysis by nucleotide binding domain 1 (NBD1) and NBD2 control gating. R region phosphorylation on multiple sites also facilitates CFTR exit from the endoplasmic reticulum (ER) (18). The phosphorylation-dependent activation of CFTR is primarily through nine PKA phosphorylation sites, but none of these sites individually seems to be essential for CFTR regulation; also, mutating one, two, or three of them has little effect (19). CFTR is a member of the ATP-binding cassette (ABC) transporter family, but the R region is significantly longer than the

Significance

Intrinsically disordered proteins lack persistent folded structure but are abundant and critical for regulatory protein interactions. They represent a challenge to the structure/function paradigm, particularly when significant disorder remains on interaction with partners. Although many disordered protein interactions have been described, little is known about multiple interactions of hub proteins or dependence on posttranslational modifications of the interaction network from a biophysical perspective. Cystic fibrosis transmembrane conductance regulator (CFTR), the chloride channel mutated in cystic fibrosis, is controlled by a disordered, phosphorylated regulatory region. Our detailed characterizations of phosphorylation-dependent interactions of the regulatory region and structural models of its highly dynamic complexes provide direct insight into the basis of CFTR regulation and the general binding mechanisms of disordered hub proteins.

Author contributions: Z.B., M.K., P.J.T., R.A.F., R.C.F., and J.D.F.-K. designed research; Z.B., M.K., and R.M. performed research; J.R.B. and A.A.-Z. contributed new reagents/analytic tools; Z.B., M.K., and J.D.F.-K. analyzed data; and Z.B., M.K., and J.D.F.-K. wrote the paper.

The authors declare no conflict of interest.

This article is a PNAS Direct Submission.

Freely available online through the PNAS open access option.

[1]Present address: Al-Qunfudhah University College, Umm Al-Qura University, Makkah Al-Mukarramah, Saudi Arabia.

[2]To whom correspondence should be addressed. E-mail: forman@sickkids.ca.

This article contains supporting information online at www.pnas.org/lookup/suppl/doi:10.1073/pnas.1315104110/-/DCSupplemental.

corresponding linker region of any other ABC transporter homolog, suggesting that the R region has a regulatory function involving a large number of partners (3). The last 40 residues at the C terminus of CFTR also comprise an intrinsically disordered segment of the protein that, like the R region, is unique among ABC transporters but conserved in different species of CFTR. The lack of the C terminus does not affect the biosynthesis and membrane targeting, but it reduces the open probability by one-half (20). Other than kinases and phosphatases, many intra- and intermolecular partners are known to interact with the R region to modulate channel trafficking and/or gating. For instance, the adaptor protein 14-3-3, which recognizes targets often through phosphorylated motifs, plays a crucial role in CFTR trafficking (18). Reciprocal regulation of SLC26A3, a chloride/bicarbonate exchanger, and CFTR at the plasma membrane involves R region interaction with the sulphate transporter and antisigma factor antagonist (STAS) domain of SLC26A3, with phosphorylation suggested to enhance this interaction (17).

The disordered character, the fundamental role in CFTR regulation, the existence of CF-causing mutations in the R region (www.genet.sickkids.on.ca and www.cftr2.org/), the many post-translational modification sites (21), and the variety of binding partners make R region a perfect candidate for detailed investigation of the structural and dynamic characteristics of a protein hub. Such studies of the effect of various partners on R region, moreover, will provide important insights into the mechanisms by which the R region regulates CFTR. The essential interacting segments within R region and its structure in the context of full-length CFTR and other partner-bound complexes are currently open questions. Here, we use primarily NMR approaches to investigate and characterize the R region in intramolecular interactions with NBD1, NBD2, and the C terminus of CFTR as well as intermolecular interactions with the SLC26A3 STAS domain and 14-3-3β. This study provides a detailed characterization of a hub protein participating in multiple dynamic complexes. Results show multiple, often overlapping R region segments that interact with these partners, consistent with a role in integrating regulatory signals, and phosphorylation dependence of interactions, suggesting a control mechanism for the R region hub.

Results

R Region Binds Multiple Partners in a Phosphorylation-Dependent Manner. To characterize the R region interactions in the CFTR interacting network (22) and probe the phosphorylation dependence of binding, HNCO NMR experiments were performed on highly PKA-phosphorylated and nonphosphorylated human CFTR R region (aa 654–838; ^{15}N,^{13}C-labeled) in the presence and absence of unlabeled binding partners. These partners included human CFTR NBD1, NBD2, and the disordered C terminus of CFTR as well as the SLC26A3 STAS domain and the human 14-3-3β protein, with the NBD constructs optimized for solubility (*Materials and Methods*). Comparison of R region HNCO spectra in the presence and absence of the partners shows that binding leads to, in general, relatively minimal chemical shift changes, with much more significant effects on the intensities of the NMR resonances (Fig. 1) and their line shapes (Fig. S1). These spectral effects are likely caused by a combination of larger apparent tumbling time of the complex (τ_c) and chemical exchange in the bound state as well as the lack of dramatic disorder-to-order transition (detailed below). Binding profiles indicate that NBDs interact more strongly with the nonphosphorylated R region, that the C terminus of CFTR and 14-3-3β preferentially interact with the PKA-phosphorylated R region, and that the STAS domain interacts similarly with both states, showing a subtle enhancement of binding for the phosphorylated R region. The binding data for the CFTR NBD2 and C terminus provide evidence for these intramolecular interactions, which have not been previously described. A control experiment was performed with human ubiquitin, showing no R region spectral changes and the specificity of these interactions (Fig. S1 *F* and *G*).

NMR Evidence for Dynamic Complexes. To better understand the NMR results, it is valuable to consider the expected effects of binding on NMR spectra. For folded proteins, with the combined molecular weights of the two partners larger than for the free protein, the folded complex tumbles more slowly in solution with a larger rotational correlation time (τ_c), giving rise to greater NMR relaxation losses and broader resonances. For intrinsically disordered proteins, the free state resonances are usually very narrow because of rapid, nearly independent motion for each residue, resulting in small τ_c values. On binding to a partner, multiple scenarios are possible. If an overall disorder-to-order transition occurs, the effective τ_c values will be significantly increased and relatively uniform, giving rise to broader resonances with similar line shapes and intensities. Such effects on the resonances were not observed for the R region binding to any of the five partners investigated. Instead, some resonances broaden, a small number disappears, and others become sharper with significant heterogeneity of intensities (Fig. 1), which is diagnostic of short segments of the disordered protein interacting with the partner and no overall disorder-to-order transition. Broadening can be thought of as having two dominant contributions. The first contribution is from the larger apparent tumbling times (τ_c) in a local residue-specific manner, because the individual segments tumble with the molecular weight of the binding partner or in larger segments caused by transient intramolecular contacts. The second contribution is the chemical exchange component of the R_2 relaxation caused by millisecond to microsecond motion from transient intra- and intermolecular interactions in the bound state or, for binding that is not fully saturated, millisecond to microsecond timescale interconversion between free and bound states. Sharpening of resonances on binding can be caused by a loss of intramolecular interactions present in the free protein that lead to broadening and line shape variability (Fig. S2 *C* and *D*) without stabilizing intermolecular interactions (both τ_c and chemical exchange contributions). In particular, the increase of intensity around residue 790 on binding to multiple partners points to loss of intramolecular interactions with this region, which was strongly suggested by paramagnetic relaxation enhancement data for the S-(2,2,5,5-tetramethyl-2,5-dihydro-1H-pyrrol-3-yl)methyl methanesulfonothioate (MTSL)-labeled R region at residue 789 that showed contacts between this site and sites of intramolecular R region binding (Fig. S2*I*).

Chemical shift perturbations are commonly used as evidence for interaction, because chemical shifts are very sensitive indicators of the ensemble averaged local electrochemical environments that are expected to change on binding. In dynamic complexes, the direct interaction sites are expected to have transient restricted motion, with the rest of the chain having minimal loss of flexibility. In such complexes, therefore, chemical shift perturbations for resonances of the unbound residues can be very small or negligible, which was observed for most of the R region interactions (Fig. 1). The directly interacting residues will have chemical shift perturbations; however, depending on the fractional population of the interacting state within the dynamic complex and the secondary structures averaged as well as the degree of resonance broadening, these perturbations are often hard or impossible to detect. Therefore, in dynamic complexes, plots of ratios of resonance intensities in the presence and absence of a binding partner as a function of residue, referred to here as binding profiles, provide a convenient measure of the interaction. Here, we describe the NMR results in detail for each partner.

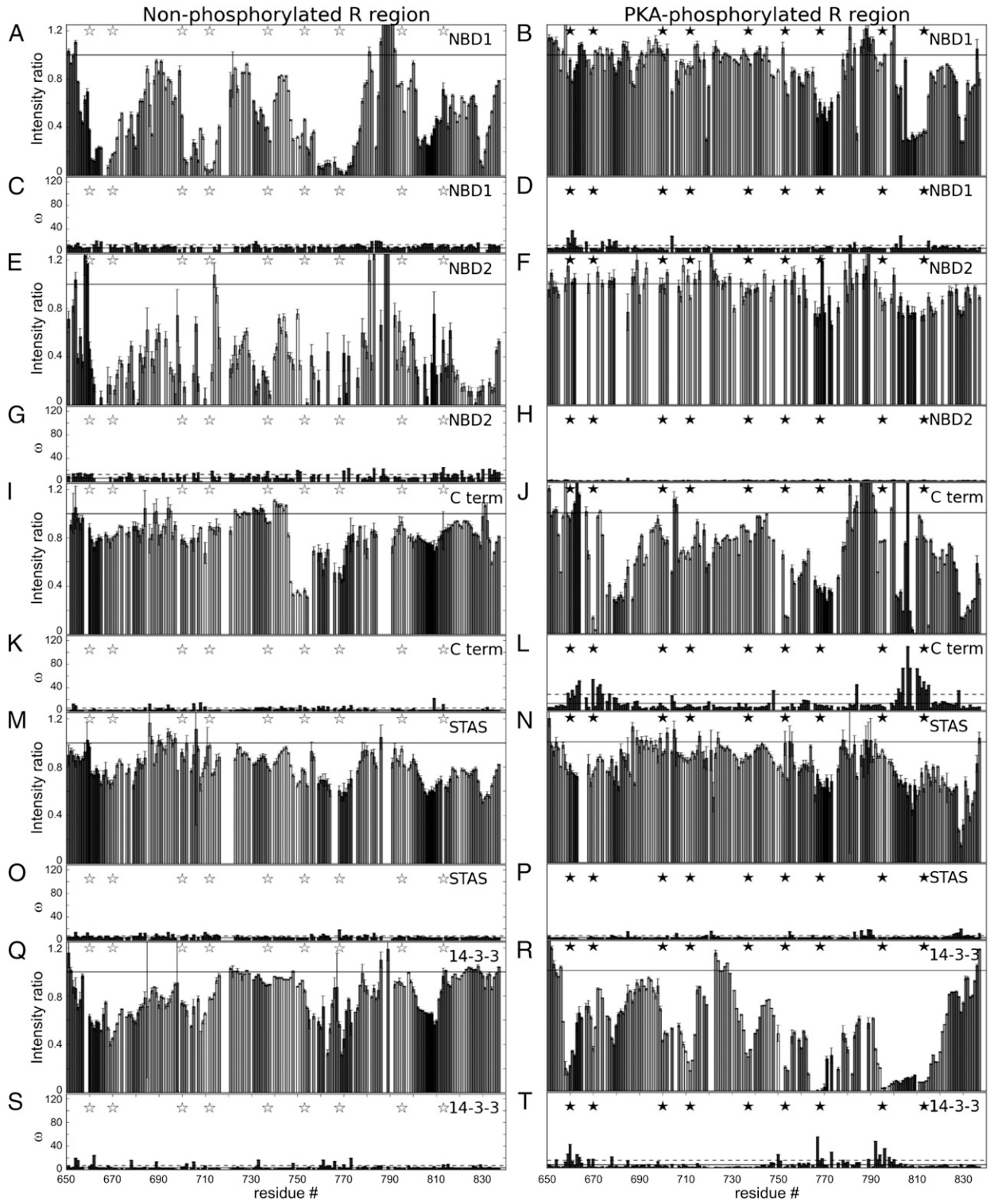

Fig. 1. R region binding profiles and chemical shift perturbations on binding. Intensity ratios and combined ^{1}H, ^{13}C, and ^{15}N chemical shift changes in Hertz of nonphosphorylated and PKA-phosphorylated ^{15}N,^{13}C-labeled R region in the presence and absence of various unlabeled binding partners. (*A*–*D*) CFTR NBD1, (*E*–*H*) CFTR NBD2, (*I*–*L*) CFTR C terminus, (*M*–*P*) SLC26A3 STAS domain, and (*Q*–*T*) 14-3-3β. On binding profile plots, solid lines represent the value one (the baseline expectation for no binding with no intensity change). Bars are colored according to the second structure propensities (Fig. S2 *A* and *B*) from most helical (black; 39% helical for nonphosphorylated and 30% helical for phosphorylated R region) to most extended structure (white; 29% extended for nonphosphorylated and 35% extended for phosphorylated R region). Maximal values of the sharpened residues around 790 reach (*A*) 2.5 on plot and (*J*) 1.8 on plot. On chemical shift perturbation plots, the solid line represents the average value, and the dashed line corresponds to a value plus 1 SD from the average. Not all residues were included in our analysis; missing are prolines, residues lacking assignments, and residues not resolved in the NMR spectra. PKA phosphorylation sites are marked as stars (open for the nonphosphorylated state and gray for the phosphorylated state).

R Region Interaction with NBD1. Binding was probed using human CFTR NBD1 (aa 387–646, Δ405–436), with a deletion of the regulatory insertion (RI) to optimize solubility and enable these biophysical studies (referred to hereafter as NBD1). The binding profile of the nonphosphorylated R region to the NBD1 (Fig. 1*A*) indicates five distinctly broadened segments (aa 661–681, 702–718, 748–778, 803–813, and 829–834) that reduce to three segments (aa 748–778, 805–815, and 829–833) showing much less broadening on phosphorylation (Fig. 1*B*). Interestingly, the three longest binding segments in the nonphosphorylated R region contain two phosphorylation sites at similar relative positions, and the hydrophobic character within the R region correlates with the PKA phosphorylation sites as well as predicted NBD1 binding elements (Fig. 1*A* and Fig. S2 *E* and *F*). Each binding segment has a phosphorylation site close to the start (aa 660, 700, and 753) and in the middle (aa 670, 712, and 768), and these longest binding segments weaken or completely vanish on phosphorylation. The observed broadening increases on the addition of a partner approaching saturating levels of binding (Fig. S3*A*), arguing that the dominant exchange is not between free and bound states but indicative of millisecond to microsecond motion within the bound state. The minimal loss of fast timescale motion on binding is shown by heteronuclear NOE experiments (Fig. S4).

In previous work (23), we described the R region binding profile for mouse NBD1 containing the RI, which is very similar but not identical to the profile for human NBD1 lacking the RI presented here (Fig. S5). We showed that many of the R region residues involved in the interaction with NBD1 in the nonphosphorylated state had significant helical propensity (Fig. S2*A*) and hypothesized that helical structure is stabilized by the interaction with NBD1. Here, we provide strong evidence for this previous hypothesis using a deuterated R region sample. The different relaxation properties of the deuterated R region reduce the broadening caused by τ_c effects and enable observation of chemical shift perturbations for resonances that are completely broadened in the protonated R region sample (Fig. 2). Note that both samples contain protonated NBD1 at nearly the same R region binding saturation levels (^{1}H: 98.3%; ^{2}H: 96.7%). In the deuterated sample, the small, although significant, nitrogen chemical shift changes of the interaction segments indicate enhanced helical conformations within the bound state. Noninteracting residues show enhanced extended conformation, with this effect being more significant in the protonated than the deuterated complex. Both the helical propensity in the free state and NBD1 binding are reduced on phosphorylation (Fig. 1*B* and Fig. S2*B*), impeding observation of the bound state chemical shifts. The helical character of the N-terminal segment of R region [regulatory extension (RE)] was also captured in NBD1 X-ray structures (Fig. S6 *A* and *B*). CD measurements are consistent with a small increase of helical structure on complex formation, because molar ellipticity values at the two characteristic helix wavelengths (208 and 222 nm) indicate enhanced helical character as a function of the protein concentration (Fig. S7).

Although R region binding to NBD1 seems to involve multiple segments, tryptophan fluorescence data can be fit adequately with single site models (Fig. S8), likely because of the two NBD1 tryptophan residues reporting on overall effects of R region binding rather than direct contact with the rings. Nonphosphorylated R region binds to NBD1 with an apparent overall K_d value of 7.1 ± 2.7 μM. This global affinity level (low micromolar) is consistent with transient interactions that are often critical for regulatory function (24), but the interaction is likely tighter in full-length CFTR, where the R region is covalently linked immediately C-terminal to NBD1. Interestingly, the K_d value of 7 μM is in the range of values calculated by fitting NMR binding profiles as a function of NBD1 concentration for the most broadened segments (Fig. S3), providing a crude measure of variation in local binding affinities across the R region. Individual binding segments within the R region do not act additively but synergistically as a domain. The interaction between phosphorylated R region and NBD1 is more than four times weaker, with a K_d value of 28.9 ± 3.4 μM.

R Region Interaction with CFTR NBD2 and C Terminus. Binding was also probed to human CFTR NBD2 using a construct containing five solubilizing mutations (aa 1193–1445, Q1280E; Y1307N;

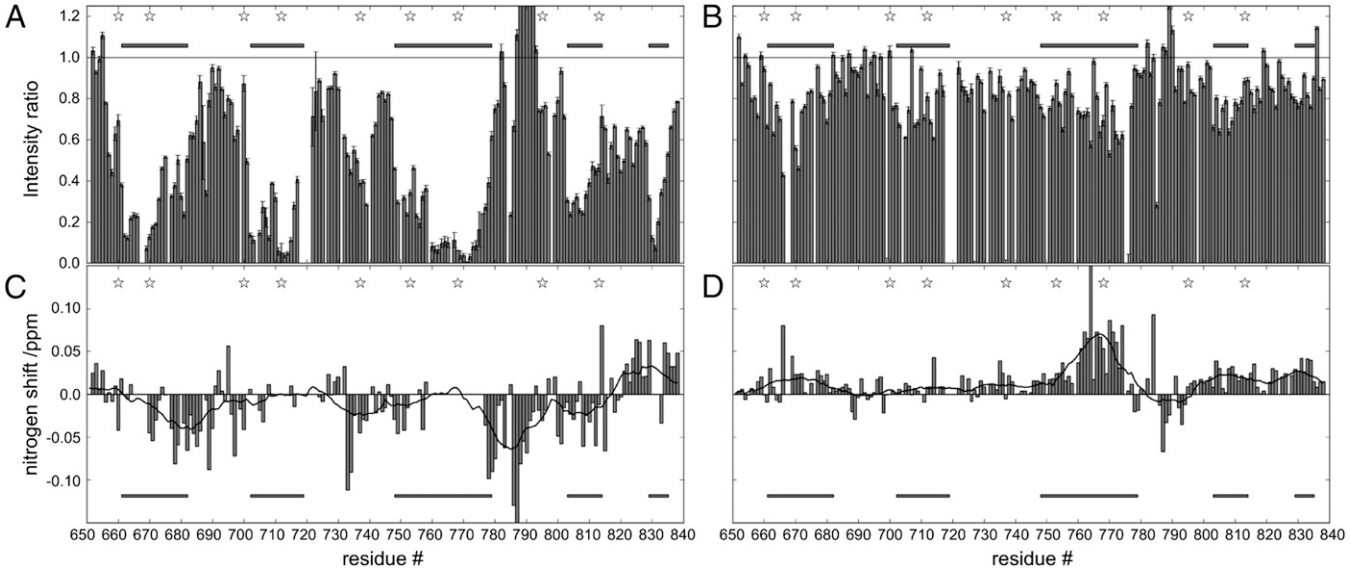

Fig. 2. NBD1 binding to protonated and deuterated nonphosphorylated R region. (*A* and *B*) R region binding profiles and (*C* and *D*) nitrogen chemical shift perturbations on binding NBD1 to (*A* and *C*) protonated or (*B* and *D*) deuterated R region. (*C* and *D*) For chemical shift perturbations, positive values correspond to increases in fractional sampling of helical conformations, whereas negative values represent enhanced extended conformations. The solid lines in *C* and *D* correspond to the trend lines using Savitzky–Golay filtering with a cubic polynomial and window size of 25. Horizontal bars indicate the R region interaction segments to NBD1 determined using a protonated R region sample (Fig. 1*A*). PKA phosphorylation sites are marked as stars.

Q1411D; L1436D; and H1402A) designed by SGX Inc. We find similar patterns of R region binding to NBD2 as for NBD1 (Fig. 1*E*), identifying NBD2 as a direct binding partner for R region and implying that the NBDs have similar binding properties. We observed at least three broadened segments (aa 661–673, 752–778, and 819–836) of the nonphosphorylated R region that reduce to one more weakly broadened segment (aa 802–824) on phosphorylation (Fig. 1*F*).

Binding of a 42-residue C-terminal peptide from human CFTR (aa 1438–1480) to nonphosphorylated R region yields a binding profile with one predominant (aa 748–771) and three more weakly broadened segments (aa 663–680, 697–717, and 803–815) (Fig. 1*I*). This interaction, like the interaction with NBD2, has not been previously reported. Binding is greatly enhanced by PKA phosphorylation with additional broadened segments (aa 669–695, 708–723, 750–778, 802–810, and 827–836) (Fig. 1*J*). Although the other interacting partners do not cause large chemical shift perturbations of R region peaks, binding of the C terminus to the phosphorylated R region does (Fig. 1*L*), implying a more significant disorder-to-order transition in R region and/or the C-terminal peptide.

Intermolecular R Region Interactions with SCL26A3 STAS Domain and 14-3-3β. CFTR channel gating is influenced by several membrane proteins, particularly the chloride-bicarbonate exchanger SLC26A3. The reciprocal regulation between SLC26A3 and CFTR involves interaction between the STAS domain and R region causing simultaneous augmentation or diminution of ion transport in both proteins (17). The binding profiles for both states of R region to human SLC26A3 STAS domain (aa 509–741) show a similar pattern (Fig. 1 *M* and *N*) with four segments broadened (aa ~660–681, ~750–777, ~805–814, and ~829–836). Our measurements agree with the previous finding that phosphorylation only slightly enhances the interaction (17).

CFTR trafficking is regulated by direct 14-3-3 binding (including to the R region) (18), providing a mechanism for R region dependence of CFTR trafficking (25). Nonphosphorylated R region binds to the human 14-3-3β at five segments (aa 656–680, 700–712, 756–766, 769–778, and 803–812) (Fig. 1*Q*). In contrast, phosphorylated R region is broadened at eight shorter segments (aa 658–667, 675–685, 698–706, 708–715, 732–744, 751–757, 764–774, and 793–821) (Fig. 1*R*). Interestingly, each segment except 675–685 contains at least one phosphorylation site located in the N-terminal half of the bound segment. This binding pattern is consistent with previously described preferences for 14-3-3 recognition (10), although none of the consensus sequences of the 14-3-3 recognition modes (24) are found exactly in R region. The absence of consensus sequences suggests relatively weak individual segment binding affinity, with the large number of nonconsensus sites increasing the interaction. There is a variation in broadening observed for different phosphorylated motifs that can be interpreted as roughly proportional to the fractional population of 14-3-3 bound states, reflecting differential local binding affinities (18). There are some small chemical shift changes, particularly for the phosphorylated R region, on 14-3-3 binding in addition to the broadening, consistent with the observation of both broadening and chemical shift changes in spectra of 14-3-3 on R region binding (18). Using fluorescence, we determined an overall K_d value of 5.4 ± 1.0 μM for interaction of phosphorylated R region with 14-3-3β (Fig. S8). Binding of nonphosphorylated R region is weaker with a K_d value of 34.3 ± 7.4 μM. These results agree with recent observations that both states interact with the 14-3-3β protein, with phosphorylated R region having greater affinity (18). Heteronuclear NOE experiments showed that PKA-phosphorylated R region binding to 14-3-3β does not significantly change the flexibility of the noninteracting R region segments, which is similar to the nonphosphorylated R region:NBD1 interaction (Fig. S4).

In the case of binding of phosphorylated R region to 14-3-3β (to 99.9% saturation), the broadening clearly involves conformational exchange of multiple, directly interacting short extended segments in addition to τ_c effects because of binding the 56.1 kDa 14-3-3β dimer. Based on these results, we have modeled the dynamic interaction of the phosphorylated R region with 14-3-3β using the structure of the ζ-isoform of human 14-3-3 [Protein Data Bank (PDB) ID code 1IB1] (26) and an isolated R region chain. Different phosphorylation sites of R region were

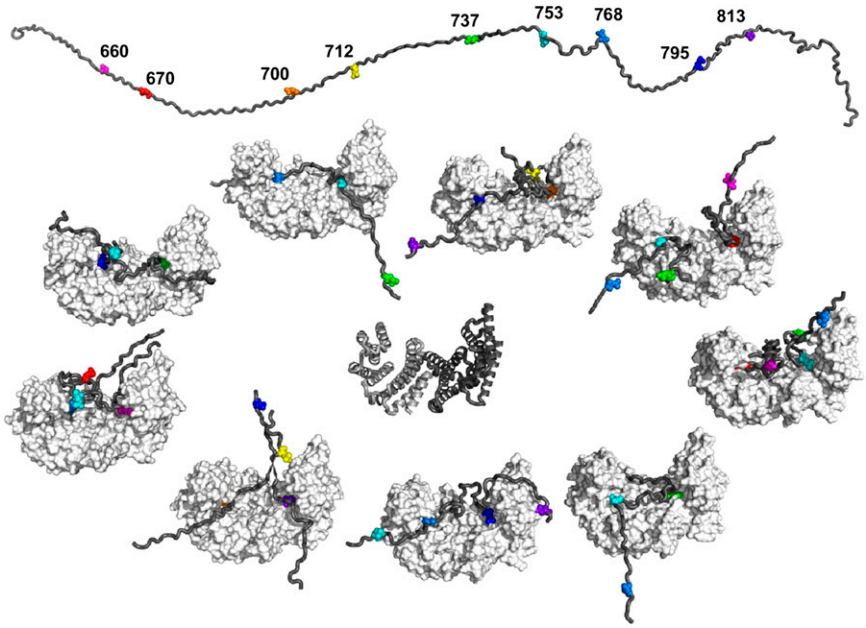

Fig. 3. Ensemble model for R region interaction with 14-3-3β. The structure of the 14-3-3β homodimer, rendered in ribbon and surface representation (gray), in a complex with PKA-phosphorylated R region (black), showing randomly selected conformers. PKA phosphorylation sites are colored in rainbow colors.

docked into the two 14-3-3 binding pockets (one for each of the monomers found within the 14-3-3 dimer). A set of models representing the variety of bound conformations of R region is presented (Fig. 3). There is variation in broadening observed for different phosphorylated motifs that can be interpreted as roughly proportional to the fractional population of 14-3-3 bound states, reflecting differential local binding affinities (18).

R Region Segments Interact with Multiple Sites on NBD1. To define the R region-interacting surfaces on NBD1, we performed TROSY (transverse relaxation-optimized spectroscopy)-HSQC (heteronuclear single quantum coherence) NMR experiments on ^{15}N-labeled NBD1 in the presence and absence of the unlabeled, nonphosphorylated R region. Comparison of the NBD1 spectra (Fig. 4) shows that R region binding causes moderate, but significant, chemical shift changes throughout NBD1 (Fig. 4*B*) using previously obtained assignments for NBD1 (27). These wide-spread chemical shifts are likely because of the shallow energy landscape of NBD1 that facilitates allosteric effects caused by the binding (27, 28), and they are difficult to simply interpret in terms of direct contacts. Resonance broadening, however, is localized primarily to two distinct sites around residues 593 and 618, suggesting that these represent effects of direct interaction (Fig. 4*A*). The surface around residue 618 (Fig. 4*A*, zone 1) is located on the likely NBD heterodimerization interface facing NBD2. The surface around 593 (Fig. 4*A*, zone 3) is located on an NBD1 surface distinct from the NBD heterodimerization interface. Significant broadening was observed around residue 549 (Fig. 4*A*, zone 2), which is also located on the dimerization interface of NBD1; however, the large number of unresolved resonances of residues from this area makes this less obvious. The fact that R region interacts with NBD1 at sites (zones 1 and 2) that were captured in NBD1 X-ray structures containing the beginning of the R region (the RE) (Fig. S6) supports the relevance of these binding sites detected as well as the use of isolated R region in our binding experiments.

Modeling of R Region Within the Context of Full-Length CFTR. EM data (29–31) do not provide detailed information on interactions with R region, making it challenging to address the structural implications of phosphorylation on the full-length protein. In addition, there is debate regarding the position of R region with respect to other domains of CFTR based on modeling (32, 33). Using our NMR binding information obtained on isolated domains of CFTR, we performed computational modeling to provide a structural view of full-length CFTR in the nonphosphorylated state. We generated a homology model of nonphosphorylated CFTR, including the NBDs, the intracellular domains (ICDs), and the transmembrane domains (TMDs), based on the crystal structure of mouse P-glycoprotein (PDB ID code 3G60; 38% identical or highly similar residues to CFTR) (34), in which the NBDs are separated to some degree, consistent with the expectation that the NBDs should not be tightly dimerized in the nonphosphorylated state. Our goal was to generate a set of models of CFTR in the closed channel state that is consistent with geometric constraints and our experimental data and that illustrates the dynamic nature of R region interactions with the NBDs. In particular, we focused on three elements of R region, for which chemical shift data show the highest fluctuating helical propensity (23) and broadening data show significant interactions with both NBD1 and NBD2 (Fig. 1). We restrained these elements to sample helical structure and sample direct interactions with various zones of NBD1 and/or NBD2 in a probabilistic fashion. The direct interaction sites were zones 1 and 2 on NBD1 and the homologous position of zone 3 on NBD2 (Fig. 4 shows detailed descriptions of interaction zones). We modeled the RI and the N and C termini as disordered with no restraints.

Fig. 5 shows 5 selected CFTR models from ∼200 models generated, showing the variety of states with up to three helical elements formed and R region interactions to NBD1, NBD2, or both (Movie S1). There are examples having zero, one, or two helical R region elements between the NBDs, showing that two NBDs in the closed channel state could be separated enough to accommodate R region acting as a physical block to heterodimerization. Importantly, R region in these models is capable of simultaneous interactions with NBD1, NBD2, and the N and C termini, and it can interact simultaneously with the NBDs and other partners, which was evident by the extended conformations possible for R region with no significant contacts to the rest of

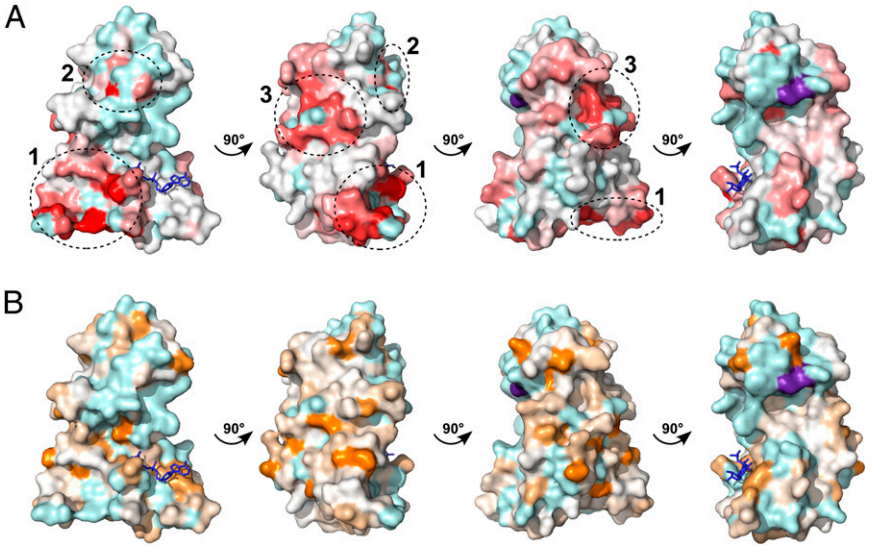

Fig. 4. Nonphosphorylated R region binding to NBD1. (*A*) Resonance intensity reductions and (*B*) chemical shift changes for ^{15}N-labeled NBD1 on binding to unlabeled R region plotted as a color gradient (PDB ID code 2PZE) (43) from intense color to white (from largest effect to no effect, respectively). Pale cyan indicates residues with no assignments or for which resonances were not resolved on the spectrum. The position of F508 is marked as purple, whereas ATP is indicated in blue. The orientation of the first surface model is from the NBD2 perspective (i.e., looking head on to the heterodimer interface). The three zones displaying significant broadening are highlighted (dashed circles).

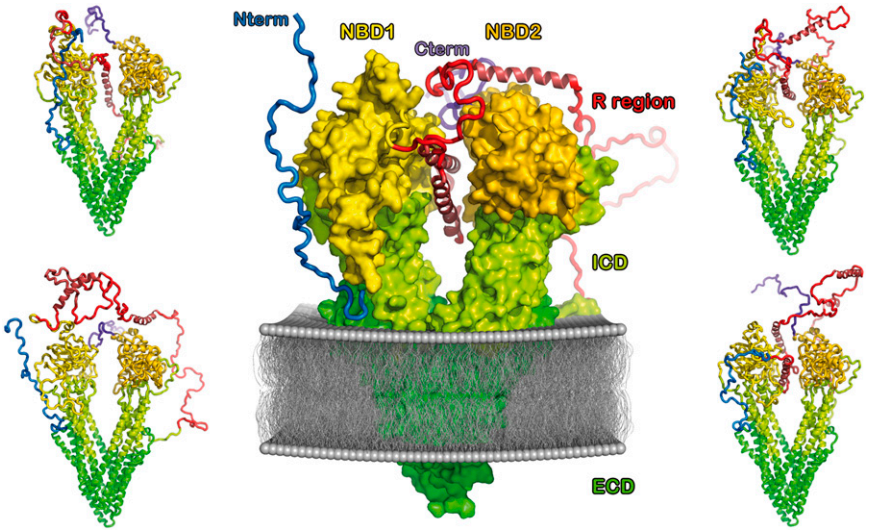

Fig. 5. Structural models of full-length CFTR in the nonphosphorylated R region state representing a closed channel state and showing five selected conformers. The N terminus is in blue (aa 1–47), TMDs and the extracellular domain (ECD) are dark green (aa 48–148, 195–241, 308–350, 860–932, 991–1034, and 1103–1149), ICDs are light green (aa 149–194, 242–307, 351–383, 842–859, 933–990, 1035–1102, and 1150–1192), NBD1 is yellow (aa 384–643), NBD2 is gold (aa 1193–1443), C terminus is purple (aa 1444–1480), and R region is red (aa 644–841).

CFTR. In agreement with the various conformations of R region in our ensemble model of CFTR, EM gold-labeling data (30) may be consistent with multiple locations of residue 696 of R region, including near the NBD:ICD interfaces. These calculated models illustrate the multiple conformations that the nonphosphorylated R region could sample, leading to significant overall structural heterogeneity within the context of the full-length CFTR.

Discussion

In this study, we provide a detailed biophysical characterization of a disordered hub region of a protein that forms dynamic complexes, revealing that CFTR R region displays different binding modes to various partners. These modes include interactions with short linear motifs, such as for the interaction with 14-3-3, or longer helical recognition elements, such as for the binding segments to NBD1. Nevertheless, many of the partners show very similar binding profiles, and most binding segments overlap with the phosphorylation sites. The lack of significant chemical shift changes observed on binding (except for binding of phosphorylated R region to the C terminus) supports the lack of dramatic disorder-to-order transitions, allowing individual segments to behave independently without long-range ordering. Thus, a static structure for R region is incompatible with its functional and binding roles, and a heterogeneous ensemble view is, instead, more appropriate. The models presented in Fig. 5 and Movie S1 give a representation of this dynamic view for the case of the nonphosphorylated closed channel state of CFTR that is consistent with our binding data and the literature as well as the accessibility of R region to other regulatory partners. Therefore, these models provide insights into the structural basis of CFTR regulation by the R region. Our current NMR data provide unique, residue-specific information on R region interactions, showing that this region remains largely disordered within the context of interactions with biological partners (Fig. S4) and that multiple segments are involved in the interactions (Fig. 1). The complexes seem to be dynamic (fuzzy) and are characterized by interconversion between multiple binding modes.

The unique role of the R region in the regulation of CFTR is most compatible with the formation of dynamic complexes. Despite the fact that R region interacts with all examined biological partners at multiple sites (control shown in Fig. S1 *F* and *G*), the affinities of the resulting complexes with NBD1 or 14-3-3 (as well as for other partners, which are inferred by comparison) are moderate. The similar, often overlapping binding segments with the overall moderate affinities suggest significant off rates that facilitate switching of partners (35) and the possibility that these partners compete with each other for R region and/or bind simultaneously. Because the R region chain outside the interaction segments remains flexible in partner-bound states, which was shown by heteronuclear NOE data (Fig. S4), each binding segment can sample various conformations and engage with partners independently, even in complex with another partner. Although our structural and interaction data were derived from isolated R region and NBDs, suggesting that increased local concentration within full-length CFTR may enhance binding, the functional demands of the R region hub for broad conformational sampling argue that our models portray a realistic picture of this dynamic protein. In addition, PKA and PKC kinases can phosphorylate R region at more than 10 sites, and our data revealed that partner binding is highly phosphorylation-dependent. Consequently, different phosphorylation states of R region are fine tuned for partner sensing, and different segments of the R region have evolved to sense and integrate signals from various sources to regulate CFTR.

The observed binding profiles are in good agreement with previous mutation and deletion studies (16), including the finding that elimination of R region leads to constitutive channel activity. The longest and strongest binding segment of R region for NBD1 comprises residues 748–778, consistent with data showing that lack of segment 760–783 also results in a constitutively active channel (36). The phosphorylation dependence of the binding supports the model, which is shown in Fig. 5 and Movie S1, that nonphosphorylated R region interacts primarily with the NBDs and inhibits their dimerization and channel activation, with phosphorylation shifting an underlying conformational equilibrium to a state in which R region binds other partners, facilitating NBD dimerization, ATP hydrolysis, and channel opening. The role of phosphorylation in shifting the conformation equilibrium rather than a large switch is further supported by the slight difference between the nonphosphorylated and the PKA-phosphorylated R region binding to STAS domain. This view of phosphorylation of R region as primarily removal of an

inhibitory interaction to heterodimer formation has been complemented by experiments revealing that PKA phosphorylation also stimulates activity by increasing R region binding to other parts of CFTR (37). Our data unify the general understanding of the role of phosphorylation by showing that phosphorylation suppresses R region:NBD interactions but enhances R region binding to the C terminus, an interaction identified in this study. One notable observation from this work is that binding of R region to all its partners leads to significantly more R region broadening than chemical shift changes, with the exception of the C terminus peptide binding to the phosphorylated R region case. This observation suggests that R region interactions are, for the most part, highly dynamic but that the binding to the C terminus may give rise to at least transient ordering of parts of R region and/or C terminus within the context of their interaction, which is potentially involved in stimulating NBD dimerization and CFTR channel function. Additional studies are required to explore whether this stimulatory R region binding in the phosphorylated state may also involve the N terminus or the ICDs in addition to the C terminus to present a more plausible model of CFTR phosphorylated on the R region representing a channel open state. The modest decrease in R region affinity for NBD1 on phosphorylation and the fact that R region interacts at sites on NBD1 outside the dimerization interface (Fig. 4) along with the presence of conformers in our model with no block of the heterodimer interface support the notion that phosphorylation is not a simple switch to enable heterodimerization but that it shifts an underlying NBD dynamic equilibrium and facilitates interaction with the C terminus and other partners.

In our previous study (23), we suggested that the binding elements in R region for mouse NBD1 are likely to be fluctuating helical elements stabilized on binding and that PKA phosphorylation decreases the probability of these transient helical structures. Here, we showed that R region binding to human NBD1 also involves five segments of R region that interact with two primary sites on the NBD1 surface in a helical conformation, overlapping those surfaces identified as interacting in crystal structures of NBD1 containing the RE, the first 30 residues of the R region (Fig. S6). These results support the relevance of the two different binding modes of the N terminus of the R region captured in crystallization studies rather than their being crystallization artifacts. In addition, our data show that these interfaces as well as another site on NBD1 not overlapping the NBD heterodimer interface can be sampled within the dynamic R region:NBD1 complex. The fact that there are five interacting segments of the R region and only three interacting surfaces on NBD1 further supports the model of a dynamic complex.

Our general observation that both partners of the NBD1:R region complex have measurable resonance broadening localized to discrete sites with minimal or delocalized chemical shift changes suggests that, in dynamic complexes, peak intensity is a more reliable probe to detect interaction sites than chemical shifts. One explanation for this observation is that the number of sampled conformations is large and that the contribution of any given individual bound conformation to the averaged chemical shift is likely to be negligible. Using loss of intensities caused by broadening as a function of concentration, we were able to calculate approximate local binding affinities (Fig. S3) that are generally consistent with the measured global binding affinities. Use of deuteration can be valuable for observing chemical shift perturbations in these dynamic complexes, because shifts indicative of helical stabilization could be observed for binding of NBD1 to deuterated R region (Fig. 2).

During CFTR trafficking, phosphorylation-dependent interactions with 14-3-3β and ε facilitate CFTR exit from the ER (18). The binding profile of the phosphorylated R region in the presence of 14-3-3β shows interaction at all of the phosphorylated serines, although none of the sequences around the serines are exact matches to consensus 14-3-3β recognition motifs (24). The multivalent binding of individually weak motifs as portrayed in our ensemble of models for this interaction (Fig. 3) likely enhances affinity. Such a scenario is reminiscent of the multivalent interaction of short phosphorylated motifs of the disordered cyclin-dependent kinase inhibitor Sic1 for the Cdc4 subunit of the SCF ubiquitin ligase (38, 39), creating a switch-like ultrasensitive degradation response to phosphorylation. In the case of R region interaction, in contrast, because of its large number of binding partners, multivalent binding of individually weak sites may facilitate rapid exchange between free and bound states to allow R region to engage with other intramolecular or intermolecular partners and generate a graded or rheostat-like response to phosphorylation.

Interactions of intrinsically disordered proteins can involve short extended peptide-like motifs, such as for Sic1:Cdc4 interactions (39) and R region binding to 14-3-3β, or longer helical binding elements (40), which seem to be more common in the case of R region. These longer binding elements are consistent with the output of computational algorithms that predicts binding sites within R region (Fig. S2). All three tested algorithms predict more than one interacting site, consistent with our interpretation of the broadening data as multivalent direct binding. Interestingly, the ANCHOR (9, 41) prediction is almost identical to the experimentally observed binding profile for nonphosphorylated R region to the NBD1 (Fig. S2*F*). Because these prediction algorithms suggest interacting elements without knowledge of the binding partners, the predictions assume that many partners should interact with the same elements. This assumption is in agreement with our experimental data showing very similar binding profiles for many of the partners, including NBD1, NBD2, and the SLC26A3 STAS domain; however, this binding mechanism is not totally general, which the 14-3-3 binding data show (Fig. 1). Such a scenario also suggests a competition among the partners.

Overlapping binding segments are common in hub proteins, which have roles of either connecting biological modules to each other or forming scaffolds that assemble functional modules, and hubs are often fully or partially disordered. The moderate- or low-affinity complexes generated by binding of such hub proteins have fast on and off rates, facilitating dynamic interactions and exposing the disordered polypeptide chain to enzymes responsible for regulatory posttranslational modifications, such as phosphorylation (42), to enable integration of multiple signals from different pathways. The complexity of CFTR trafficking and function is currently not understood at the molecular level, but our studies defining phosphorylation-dependent binding involving multiple interacting segments of R region for multiple intramolecular and intermolecular partners begin to provide insights. Competition between binding of the same elements among the various binding partners, which involves transient interaction at multiple sites, likely enables the regulatory region to act as a dynamic integrator to control CFTR gating and trafficking. This comprehensive study of an intrinsically disordered hub protein forming dynamic complexes with many partners, including two interactions not previously described, also enables generalization about the optimal methods for the characterization of such dynamic hubs and their unique interaction properties.

Materials and Methods

Protein Expression and Purification. All proteins were expressed in BL21(DE3) CodonPlus (RIL) cells (Stratagene). The human CFTR R region (aa 654–838; F833L) was prepared as described in the work by Baker et al. (23), and the F833L polymorphism was used to optimize solubility. Human CFTR NBD1 was expressed from a pET-SUMO plasmid (Invitrogen) encoding residues (aa 387–646, Δ405–436) fused with an N-terminal His_6-smt3 (SUMO) tag and purified as described for mouse NBD1 (23) with the deletion of the largely disordered

RI required for solubility. The NBD2 domain of human CFTR (aa 1193–1445, Q1280E; Y1307N; Q1411D; H1402A; and L1436D), a construct with solubilizing mutations designed by SGX, Inc., was encoded on a pET-SUMO plasmid (Invitrogen). NBD2 was purified from the soluble fraction using a buffer containing 50 mM Tris·HCl, pH 8.0, 150 mM NaCl, 100 mM arginine, 5 mM $MgCl_2$, 2 mM ATP, 12.5% (vol/vol) glycerol, and 2 mM mercapthoethan-2-ol. The purification included an Ni^{2+} affinity chromatography followed by SUMO protease cleavage and a second Ni^{2+} affinity chromatography. The final step was size exclusion chromatography. Although it is not known whether these mutations perturb R region interaction, it was not possible to use WT protein for these biophysical studies. The C terminus of human CFTR (aa 1438–1480) was encoded on a pET-24 plasmid (Invitrogen), and a thrombin cleavage was performed to remove the tag. The STAS domain of the human SLC26A3 (aa 509–741) and human 14-3-3β were encoded on pET-SUMO plasmid (Invitrogen), and their purifications were the same as described for the NBD2 of CFTR, except with a buffer containing 50 mM Tris·HCl, pH 7.5, 150 mM NaCl, 2% (mass/vol) glycine, and 10 mM mercapthoethan-2-ol. R region phosphorylation by PKA was performed as described in the work by Baker et al. (23).

NMR Experiments. All NMR measurements were collected on a Varian Inova 800-MHz Spectrometer at 10 °C with a triple-resonance probe. Recorded data were processed using NMRPipe (44) and analyzed using Sparky (www.cgl.ucsf.edu/home/sparky/). The heteronuclear NOE (45) values were measured by recording experiments including or not including a 4-s period of ^1H saturation pulses with a 12-s total recovery delay in both cases. Paramagnetic relaxation enhancements were measured on MTSL-labeled ^{15}N,^{13}C R region mutant A789C/C833S in 125 mM KH_2PO_4, pH 6.8, 125 mM KCl, and 2 mM EDTA by measuring HNCO spectra (46) recorded with eight transients at 10 °C in both oxidized and reduced states.

R Region Interaction Experiments. Complete phosphorylation was achieved at 660, 700, 712, 737, 768, 795, and 813 sites, and partial phosphorylation (60–95%) was achieved at the monobasic sites 670 and 753 using PKA in vitro, which was monitored by MS and NMR spectroscopy (23). HNCO spectra (46) were recorded with eight transients at 10 °C on 50–150 μM ^{15}N,^{13}C-labeled R region samples in the absence and presence of unlabeled interacting partners. NBD1 binding experiments were carried out at 430 μM concentration (8× molar excess) in 50 mM NaH_2PO_4, pH 7.0, 150 mM NaCl, 5 mM $MgCl_2$, 5 mM ATP, 5 mM DTT, 2% (vol/vol) glycerol, 5 mM benzamidine, and 10% (vol/vol) D_2O. NBD2 binding was measured at 360 μM (9× molar ratio) in 20 mM Hepes, pH 7.2, 100 mM NaCl, 5 mM $MgCl_2$, 5 mM ATP, 2 mM DTT, 4% (vol/vol) glycerol, and 10% (vol/vol) D_2O. CFTR C terminus measurements were done at 560 μM (4.5× molar excess) in 50 mM Tris·HCl, pH 7.15, 150 mM NaCl, 10 mM mercaptoethan-2-ol, and 10% (vol/vol) D_2O. STAS domain binding was measured at 320 μM (2.5× molar excess) in 50 mM Tris·HCl, pH 7.20, 200 mM NaCl, 2% (m/vol) glycine, 10 mM mercaptoethan-2-ol, and 10% (vol/vol) D_2O. Experiments on 14-3-3β protein were carried out at 300 μM (2× molar access) in a buffer of 50 mM Tris·HCl, pH 7.50, 150 mM NaCl, 2 mM DTT, and 10% (vol/vol) D_2O. Control experiment with ubiquitin was done at 250 μM (2.2× molar excess) in 50 mM Hepes, pH 7.3, 150 mM NaCl, 2 mM DTT, and 10% (vol/vol) D_2O. The chemical shift differences for HNCO resonances were calculated as $\mathrm{sqrt}((\Delta\omega_{1H})^2 + (\Delta\omega_{15N})^2 + (\Delta\omega_{13C})^2)$. To identify R region binding sites on the NBD1 surface, TROSY-HSQC (47, 48) NMR experiments were carried out on ^{15}N-labeled NBD1 in the absence and presence of unlabeled R region at 571 μM concentration (2× molar excess) in 50 mM Tris·HCl, pH 7.15, 150 mM NaCl, 5 mM $MgCl_2$, 100 mM arginine, 2 mM ATP, 2 mM DTT, 4% (vol/vol) glycerol, and 10% (vol/vol) D_2O. Deuterated R region binding measurements were acquired using ^2H,^{13}C,^{15}N-labeled R region and unlabeled NBD1 at 200 and 390 μM, respectively, in 50 mM NaH_2PO_4, pH 7.00, 150 mM NaCl, 5 mM $MgCl_2$, 5 mM ATP, 2 mM DTT, 4% (vol/vol) glycerol, and 25% (vol/vol) D_2O.

CD. CD spectra were acquired on a Jasco spectropolarimeter (810 CD Spectropolarimeter; JASCO) in a buffer of 20 mM NaH_2PO_4, pH 7.4, 20 mM NaF, and 1 mM DTT at 25 °C. Each spectrum was an average of three scans. Spectra were measured in the range of 190–250 nm in steps of 0.1 nm, with a path length of 0.01 cm (Hellma Analytics), response time of 1 s, and scan speed of 50 nm/min.

Fluorescence Measurements. Trp fluorescence measurements were carried out on an AVIV ATF-150 spectrofluorometer (Aviv Biomedical Inc.) equipped with an automatic titrator in 50 mM Tris·HCl, pH 7.50, 150 mM NaCl, 5 mM $MgCl_2$, 2 mM ATP, 5% (vol/vol) glycerol, and 2 mM DTT for NBD1 or 50 mM Tris·HCl, pH 7.50, 150 mM NaCl, and 2 mM DTT for 14-3-3β.

Computational Modeling. The protein 14-3-3 (PDB ID code 1IB1) (26) was modeled to interact with two of seven phosphate-containing motifs of the R region at a time. All possible combinations were modeled (total of 42 models) initially using CNS (http://cns.csb.yale.edu/v1.2/) starting from an extended form of R region to perform dynamics in torsion angle space, with restraints bringing the two R region sites closer to 14-3-3 (3.0 Å away from each other; upper and lower distances of 1.0 Å). Then, docking was performed using HADDOCK 2.1 (49) with default parameters.

For the model of full-length CFTR, a homology model of the TMDs, ICDs, and NBDs of the CFTR (core) was generated using a minimalist approach with alignment only of the stable secondary structural elements, facilitating flexibility in loop regions. From chain A of P-glycoprotein (PDB ID code 3G60) (34), all C_α/C_β distances were retrieved and imposed as restraints for the aligned elements using CNS along a simulating annealing protocol as defined in RECOORDS (50). Helical dihedral angles were imposed at three interacting segments (aa 659–680, 700–722, and 759–777) of R region, where NBD1 binding leads to significant broadening that is relieved on phosphorylation (Fig. 1 *A* and *B*). In total, 7,500 structures were generated (with no refinement in water). The conformer with the lowest rmsd to 3G60 was used for generating the final models. Using the Edit module of PyMol (The PyMOL Molecular Graphics System, Version 1.5.0.1; Schrödinger, LLC) to facilitate translations/rotations, the interacting segments were approximately positioned. Each of three interacting segments could interact or not with NBD1 or NBD2 at specified areas (zones) defined by the NBD1:R region interaction data. Helical conformation was only strictly restrained when the segment interacted with the NBDs. When the manipulation of some parts of R region required detaching these parts from the rest of the chain, CNS was used to reconstruct the model. For this procedure, all of the protein but the R region was first fixed in space. Then, a series of rigid body minimizations and short simulations of the side chains only (fixed backbone) was performed to avoid overlaps of the interacting regions with the core of CFTR. Finally, all of the protein was unfixed, and all C_α/C_β distance restraints were imposed again in a last Cartesian dynamics, for which the van der Waals and electrostatic energy terms were included. The membrane was generated with PyMol, and a limited number of models having steric clashes to the membrane was discarded.

ACKNOWLEDGMENTS. We thank Lewis Kay for assistance with NMR data collection, SGX Pharmaceuticals for supplying NBD2 protein and plasmid, and Jennifer Dawson and Rhea P. Hudson for assistance with protein preparation. We acknowledge Jennifer Baker, Andrew Chong, Christine Bear, Shane Atwell, and Xun Zhao for stimulating and helpful discussions. Z.B. was supported by an award from the Canadian Institutes of Health Research (CIHR) Strategic Training Program in Protein Folding and Interaction Dynamics. This work was funded by Cystic Fibrosis Foundation Therapeutics Grants FORMAN05XX0, FORD08XX0, and FRIZZE05XX0, National Institutes of Health Grant DK068196 (to R.A.F.), and a grant from Cystic Fibrosis Canada (J.D.F.-K.).

1. Ward JJ, Sodhi JS, McGuffin LJ, Buxton BF, Jones DT (2004) Prediction and functional analysis of native disorder in proteins from the three kingdoms of life. *J Mol Biol* 337(3):635–645.
2. Tompa P (2012) Intrinsically disordered proteins: A 10-year recap. *Trends Biochem Sci* 37(12):509–516.
3. Dosztányi Z, Chen J, Dunker AK, Simon I, Tompa P (2006) Disorder and sequence repeats in hub proteins and their implications for network evolution. *J Proteome Res* 5(11):2985–2995.
4. Dunker AK, Cortese MS, Romero P, Iakoucheva LM, Uversky VN (2005) Flexible nets. The roles of intrinsic disorder in protein interaction networks. *FEBS J* 272(20):5129–5148.
5. Haynes C, et al. (2006) Intrinsic disorder is a common feature of hub proteins from four eukaryotic interactomes. *PLoS Comput Biol* 2(8):e100.
6. Pancsa R, Fuxreiter M (2012) Interactions via intrinsically disordered regions: What kind of motifs? *IUBMB Life* 64(6):513–520.
7. Iakoucheva LM, et al. (2004) The importance of intrinsic disorder for protein phosphorylation. *Nucleic Acids Res* 32(3):1037–1049.
8. Galea CA, Wang Y, Sivakolundu SG, Kriwacki RW (2008) Regulation of cell division by intrinsically unstructured proteins: Intrinsic flexibility, modularity, and signaling conduits. *Biochemistry* 47(29):7598–7609.
9. Mészáros B, Simon I, Dosztányi Z (2009) Prediction of protein binding regions in disordered proteins. *PLoS Comput Biol* 5(5):e1000376.
10. Oldfield CJ, et al. (2008) Flexible nets: Disorder and induced fit in the associations of p53 and 14-3-3 with their partners. *BMC Genomics* 9(Suppl 1):S1.
11. James LC, Tawfik DS (2003) Conformational diversity and protein evolution—a 60-year-old hypothesis revisited. *Trends Biochem Sci* 28(7):361–368.

12. Boehr DD, Nussinov R, Wright PE (2009) The role of dynamic conformational ensembles in biomolecular recognition. *Nat Chem Biol* 5(11):789–796.
13. Fuxreiter M (2012) Fuzziness: Linking regulation to protein dynamics. *Mol Biosyst* 8(1): 168–177.
14. Mittag T, Kay LE, Forman-Kay JD (2010) Protein dynamics and conformational disorder in molecular recognition. *J Mol Recognit* 23(2):105–116.
15. Winter MC, Welsh MJ (1997) Stimulation of CFTR activity by its phosphorylated R domain. *Nature* 389(6648):294–296.
16. Csanády L, et al. (2000) Severed channels probe regulation of gating of cystic fibrosis transmembrane conductance regulator by its cytoplasmic domains. *J Gen Physiol* 116(3):477–500.
17. Ko SBH, et al. (2004) Gating of CFTR by the STAS domain of SLC26 transporters. *Nat Cell Biol* 6(4):343–350.
18. Liang X, et al. (2012) Phosphorylation-dependent 14-3-3 protein interactions regulate CFTR biogenesis. *Mol Biol Cell* 23(6):996–1009.
19. Ostedgaard LS, Baldursson O, Vermeer DW, Welsh MJ, Robertson AD (2000) A functional R domain from cystic fibrosis transmembrane conductance regulator is predominantly unstructured in solution. *Proc Natl Acad Sci USA* 97(10):5657–5662.
20. Ostedgaard LS, et al. (2003) Effects of C-terminal deletions on cystic fibrosis transmembrane conductance regulator function in cystic fibrosis airway epithelia. *Proc Natl Acad Sci USA* 100(4):1937–1942.
21. McClure M, et al. (2012) Purification of CFTR for mass spectrometry analysis: Identification of palmitoylation and other post-translational modifications. *Protein Eng Des Sel* 25(1):7–14.
22. Wang X, et al. (2006) Hsp90 cochaperone Aha1 downregulation rescues misfolding of CFTR in cystic fibrosis. *Cell* 127(4):803–815.
23. Baker JMR, et al. (2007) CFTR regulatory region interacts with NBD1 predominantly via multiple transient helices. *Nat Struct Mol Biol* 14(8):738–745.
24. Johnson C, et al. (2010) Bioinformatic and experimental survey of 14-3-3-binding sites. *Biochem J* 427(1):69–78.
25. Lewarchik CM, Peters KW, Qi J, Frizzell RA (2008) Regulation of CFTR trafficking by its R domain. *J Biol Chem* 283(42):28401–28412.
26. Obsil T, Ghirlando R, Klein DC, Ganguly S, Dyda F (2001) Crystal structure of the 14-3-3zeta:serotonin N-acetyltransferase complex. a role for scaffolding in enzyme regulation. *Cell* 105(2):257–267.
27. Hudson RP, et al. (2012) Conformational changes relevant to channel activity and folding within the first nucleotide binding domain of the cystic fibrosis transmembrane conductance regulator. *J Biol Chem* 287(34):28480–28494.
28. Dawson JE, Farber PJ, Forman-Kay JD (2013) Allosteric coupling between the intracellular coupling helix 4 and regulatory sites of the first nucleotide-binding domain of CFTR. *PLoS One* 8(9):e74347.
29. Rosenberg MF, et al. (2011) The cystic fibrosis transmembrane conductance regulator (CFTR): Three-dimensional structure and localization of a channel gate. *J Biol Chem* 286(49):42647–42654.
30. Zhang L, Aleksandrov LA, Riordan JR, Ford RC (2011) Domain location within the cystic fibrosis transmembrane conductance regulator protein investigated by electron microscopy and gold labelling. *Biochim Biophys Acta* 1808(1):399–404.
31. Mio K, et al. (2008) Three-dimensional reconstruction of human cystic fibrosis transmembrane conductance regulator chloride channel revealed an ellipsoidal structure with orifices beneath the putative transmembrane domain. *J Biol Chem* 283(44): 30300–30310.
32. Mornon JP, Lehn P, Callebaut I (2009) Molecular models of the open and closed states of the whole human CFTR protein. *Cell Mol Life Sci* 66(21):3469–3486.
33. Serohijos AWR, et al. (2008) Phenylalanine-508 mediates a cytoplasmic-membrane domain contact in the CFTR 3D structure crucial to assembly and channel function. *Proc Natl Acad Sci USA* 105(9):3256–3261.
34. Aller SG, et al. (2009) Structure of P-glycoprotein reveals a molecular basis for polyspecific drug binding. *Science* 323(5922):1718–1722.
35. Zor T, Mayr BM, Dyson HJ, Montminy MR, Wright PE (2002) Roles of phosphorylation and helix propensity in the binding of the KIX domain of CREB-binding protein by constitutive (c-Myb) and inducible (CREB) activators. *J Biol Chem* 277(44): 42241–42248.
36. Ostedgaard LS, Baldursson O, Welsh MJ (2001) Regulation of the cystic fibrosis transmembrane conductance regulator Cl- channel by its R domain. *J Biol Chem* 276(11):7689–7692.
37. Chappe V, Irvine T, Liao J, Evagelidis A, Hanrahan JW (2005) Phosphorylation of CFTR by PKA promotes binding of the regulatory domain. *EMBO J* 24(15):2730–2740.
38. Mittag T, et al. (2010) Structure/function implications in a dynamic complex of the intrinsically disordered Sic1 with the Cdc4 subunit of an SCF ubiquitin ligase. *Structure* 18(4):494–506.
39. Mittag T, et al. (2008) Dynamic equilibrium engagement of a polyvalent ligand with a single-site receptor. *Proc Natl Acad Sci USA* 105(46):17772–17777.
40. Sivakolundu SG, Bashford D, Kriwacki RW (2005) Disordered p27Kip1 exhibits intrinsic structure resembling the Cdk2/cyclin A-bound conformation. *J Mol Biol* 353(5): 1118–1128.
41. Dosztányi Z, Mészáros B, Simon I (2009) ANCHOR: Web server for predicting protein binding regions in disordered proteins. *Bioinformatics* 25(20):2745–2746.
42. Fuxreiter M, Tompa P, Simon I (2007) Local structural disorder imparts plasticity on linear motifs. *Bioinformatics* 23(8):950–956.
43. Atwell S, et al. (2010) Structures of a minimal human CFTR first nucleotide-binding domain as a monomer, head-to-tail homodimer, and pathogenic mutant. *Protein Eng Des Sel* 23(5):375–384.
44. Delaglio F, et al. (1995) NMRPipe: A multidimensional spectral processing system based on UNIX pipes. *J Biomol NMR* 6(3):277–293.
45. Farrow NA, et al. (1994) Backbone dynamics of a free and phosphopeptide-complexed Src homology 2 domain studied by 15N NMR relaxation. *Biochemistry* 33(19): 5984–6003.
46. Muhandiram DR, Kay LE (1994) Gradient-enhanced triple-resonance three-dimensional NMR experiments with improved sensitivity. *J Magn Reson* 103(3):203–216.
47. Zhang O, Kay LE, Olivier JP, Forman-Kay JD (1994) Backbone 1H and 15N resonance assignments of the N-terminal SH3 domain of drk in folded and unfolded states using enhanced-sensitivity pulsed field gradient NMR techniques. *J Biomol NMR* 4(6): 845–858.
48. Pervushin K, Riek R, Wider G, Wüthrich K (1997) Attenuated T2 relaxation by mutual cancellation of dipole-dipole coupling and chemical shift anisotropy indicates an avenue to NMR structures of very large biological macromolecules in solution. *Proc Natl Acad Sci USA* 94(23):12366–12371.
49. Dominguez C, Boelens R, Bonvin AMJ (2003) HADDOCK: A protein-protein docking approach based on biochemical or biophysical information. *J Am Chem Soc* 125(7): 1731–1737.
50. Nederveen AJ, et al. (2005) RECOORD: A recalculated coordinate database of 500+ proteins from the PDB using restraints from the BioMagResBank. *Proteins* 59(4): 662–672.